One-neutron stripping processes to excited states of ^{90}Y* in the ^{89}Y(^{6}Li, ^{5}Li)^{90}Y* reaction

G. L. Zhang,[1] G. X. Zhang,[1,*] S. P. Hu,[2,†] Y. J. Yao,[1] J. B. Xiang,[1] H. Q. Zhang,[3] J. Lubian,[4] J. L. Ferreira,[4] B. Paes,[4] E. N. Cardozo,[4] H. B. Sun,[2] J. J. Valiente-Dobón,[5] D. Testov,[6] A. Goasduff,[5,6] P. R. John,[7] M. Siciliano,[5] F. Galtarossa,[6] R. Francesco,[6] D. Mengoni,[6] D. Bazzacco,[6] E. T. Li,[2] X. Hao,[2] and W. W. Qu[8]

[1]*School of Physics and Nuclear Energy Engineering, Beihang University, Beijing 100191, China*
[2]*College of Physics and Energy, Shenzhen University, Shenzhen 518060, China*
[3]*China Institute of Atomic Energy, Beijing 102413, China*
[4]*Instituto de Física, Universidade Federal Fluminense, Avenida Litorânea s/n, Gragoatá, Niterói, Rio de Janeiro 24210-340, Brazil*
[5]*INFN, Laboratori Nazionali di Legnaro, I-35020 Legnaro, Italy*
[6]*Dipartimento di Fisica and INFN, Sezione di Padova, I-35131 Padova, Italy*
[7]*Institut für Kernphysik der Technischen Universität Darmstadt, Germany*
[8]*School of Radiation Medicine and Protection, Medical College of Soochow University, Soochow 215123, China*

(Received 16 October 2017; published 23 January 2018)

The measurement of one-neutron stripping cross sections for the ^{89}Y(^{6}Li,^{5}Li)^{90}Y* reaction at 22 MeV and 34 MeV is reported, using both in-beam and off-beam γ-ray spectroscopy methods. Characteristic γ lines of ^{90}Y are clearly identified by both the γ-γ and proton-γ coincidence methods. The obtained cross section of one-neutron stripping at 34 MeV is found to be much smaller than that at 22 MeV. The one-neutron stripping cross sections measured for this system have the same order of magnitude as the one measured for the same reaction for the ^{6}Li + ^{96}Zr system at energies around the Coulomb barrier. Parameter-free coupled reaction channel calculations agree quite well with the experimental data. Theoretical study of the effect of the one-neutron transfer on the elastic total fusion cross section is performed.

DOI: 10.1103/PhysRevC.97.014611

I. INTRODUCTION

In the past few years, much more theoretical and experimental research focused on reactions induced by weakly bound nuclei, especially elastic scattering, breakup, and fusion [1–8]. It is assumed that the projectile is the nucleus that is weakly bound (this is always the case when radioactive nuclei are involved, for example). In fusion reactions, when weakly bound projectiles are involved, different processes may occur. When the whole projectile fuses with the target nucleus without breakup, this process is known as direct complete fusion (DCF). After the breakup of weakly bound nuclei (we usually consider as the projectile), different processes can occur. When all the fragments fuse with the target nucleus, this process is called sequential complete fusion (SCF). When only part of the fragments fuses with the target nucleus, this process is called incomplete fusion (ICF). Experimentally, SCF and DCF cannot be separated because they have the same residues. So, complete fusion (CF) includes the SCF and DCF processes. The total fusion (TF) cross section is equal to the sum of the CF and ICF. From this, it is clear that the breakup process may compete with the fusion cross section [1–8]. Meanwhile, other direct reaction processes may also compete with and influence the fusion process, such as the collective excitation of the projectile and/or the target, the transfer of some particles or a cluster, etc.

Systematic results [9–18] have shown that the effect of the breakup plus transfer channels on the CF is to suppress it at energies above the Coulomb barrier and to produce some enhancement at sub-barrier energies when compared to coupled channel calculations that do not account for the coupling to continuum states. When the ICF cross section of part of the projectiles fragments is added to the CF, the total fusion cross sections are not suppressed at energies above the Coulomb barrier, which means that part of the flux that would produce CF actually produces ICF of the weakly bound projectile. In fact, it has been shown that the breakup process produces repulsive polarization potential that increases the fusion barrier height and consequently suppresses the CF cross section at near-barrier energies [19–21].

The behavior of the energy dependence of the obtained optical potential of weakly bound systems is different from the usual threshold anomaly [22–26], which was named the breakup threshold anomaly [27]. This phenomenon is attributed to the repulsive polarization potential produced by the breakup, which populates continuum states [20,28,29]. The same conclusions about the repulsive character of the breakup polarization potential were obtained in the analysis of fusion and quasielastic barrier distributions [30–32]. In the theoretical calculations, the breakup is usually considered as a direct process. However, from the experiment, it was observed that sequential breakup (transfer followed by breakup) might predominate over the direct breakup at energies below the

*skyzhanggx@buaa.edu.cn
†husp@szu.edu.cn

Coulomb barrier for some systems [33–36]. The direct breakup may be regarded as a one- or two-step process. One-step breakup is when the projectile breaks up without exciting resonances. When the resonance is excited, the breakup is usually called a two-step process. Two different breakup processes are identified depending on whether the projectile breaks up before it reaches to the target or when it is moving apart from the target. The first case is recognized as prompt breakup while the second is the so-called delayed breakup [34,35,37,38].

Direct transfers of neutrons and clusters of nucleons involving stable and radioactive weakly bound projectiles have been studied in the past years due to the recent comprehensive investigation of reaction mechanisms involving weakly bound nuclei [39–49]. In the literature one usually finds that the measured cross sections are only attributed to ICF and the direct transfer is neglected. However, transfer process may lead to some complications in experimental and theoretical studies of fusion. For example, for a weakly bound nucleus ^{6}Li transfer of p can produce the same nuclei as the ICF of fragments after the ^{6}Li breakup. From the experimental viewpoint, the two kinds of processes cannot be easily separated, and actually, when one reports the ICF cross sections, the results are the sum of both processes. From the theoretical viewpoint, transfer and ICF are two different processes. The former is a one-step process and the latter is a two-step process where projectiles break up and then a part of the fragments fuses with the target nucleus. At sub-barrier energies, ICF occurs after a tunneling of part of projectile whereas no tunneling is required for the direct transfer. Since direct transfer and breakup do not need to tunnel through the barrier, the excitation functions do not drop as fast as the fusion excitation function at sub-barrier energies. As a result, the cross sections of those processes may be larger than the fusion cross sections at sub-barrier energies.

This phenomenon has been observed in the one-neutron stripping of ^{6}Li + ^{96}Zr [40] and ^{9}Be [41]. One-neutron stripping and one-neutron pickup have been measured in the ^{6,7}Li + ^{198}Pt systems. For ^{6}Li + ^{198}Pt it is shown that the direct reaction cross section is much larger than the fusion cross section at energies below the barrier [42]. For ^{7}Li + ^{198}Pt it is found that the one- and two-neutron stripping and the one-neutron pickup reaction give important contributions [43]. In ^{6,7}Li + ^{197}Au collision the large transfer cross sections are observed [44]. In the investigations of ^{6,7}Li + ^{64}Zn collision, the conclusion is that CF is the main process at energies above the Coulomb barrier whereas transfer is the dominant process below the Coulomb barrier [45]. For ^{9}Be-induced reactions, very few works about transfer reactions above or below the Coulomb barrier are reported. Most of them focus on the one-neutron stripping measurements [46,47]. Transfer reactions are also important in collisions of neutron-halo nuclei such as ^{6,8}He [48–50]. From experiments, it was found that the one- and two-neutron transfer channels are the dominant processes below the Coulomb barrier and are still important at energies above the Coulomb barrier.

When the γ-spectroscopy method is used and characteristic γ lines of the targetlike nucleus are detected, the transfer processes to excited states can be reliably identified. To introduce the investigations of reaction mechanisms involving weakly bound nuclei, in the present paper we report the ^{89}Y(^{6}Li,^{5}Li)^{90}Y* transfer reaction at energies above the Coulomb barrier.

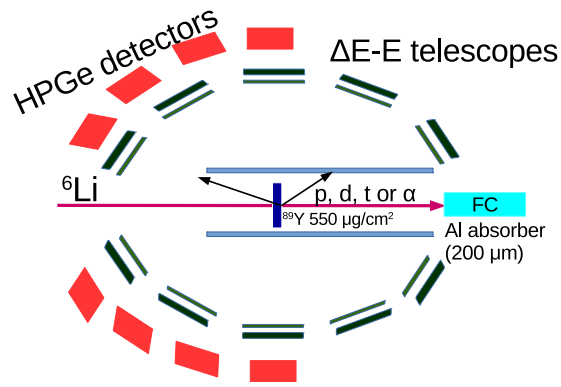

FIG. 1. The schematic of the experimental setup (sectional view). HPGe detectors and ΔE-E telescopes present the schematic of a part of GALILEO and EUCLIDES arrays, respectively. For details, see the text.

This paper is organized as follows. Section II describes the experimental procedure. The data analysis and discussions are presented in Sec. III. Section IV presents the theoretical methods and comparisons between the results of the theoretical calculations and the experimental data. In Sec. V we discuss the effect of the one-neutron stripping reaction on the elastic and total fusion cross sections. The sensibility of the obtained transfer cross section to the used form factors is also discussed in details. The summary is given in Sec. VI.

II. EXPERIMENTAL SETUP

The experiment was performed at the Tandem-XTU accelerator of Legnaro National Laboratory in Italy. The schematic of the experimental setup is shown in Fig. 1. A ^{6}Li^{3+} beam with $E_{\rm lab}$ = 34 MeV and 22 MeV and an average beam intensity of $\sim$ 0.35 pnA was impinging on an ^{89}Y target of 550 $\mu g/\text{cm}^2$ backed with a 340 $\mu g/\text{cm}^2$ ^{12}C foil. The beam flux is recorded by a Faraday cup (FC) placed 3 m behind the target. The output signals were input into the module ORTEC439, which is a digital current integrator, so that the total pulse number can be obtained. Depending on the scale of ORTEC439 module, the charge number of each pulse can be determined. Thus, the number of beam particles can be obtained.

The ^{89}Y target was placed at the center of the GALILEO γ-ray array [51] in combination with 4π Si-ball EUCLIDES [52–54], which measured the light charged particles. The GALILEO array was used to detect online γ rays emitted by the reaction products. The GALILEO array is made of 25 Compton-Suppressed bismuthgermanate high-purity germanium (BGO-HPGe) detectors distributed on four rings: ten detectors at 90°, five detectors at each of the following angles 119°, 129°, and 152°. The full-energy-peak efficiency and energy calibration of the HPGe detectors were achieved by using a set of standard radioactive sources of ^{88}Y, ^{241}Am, ^{152}Eu, ^{133}Ba, and ^{60}Co at the target position. EUCLIDES consists of 40 silicon telescopes where each single silicon telescope

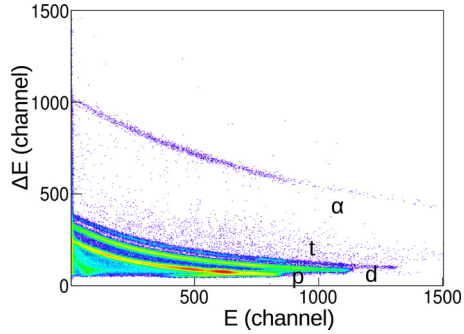

FIG. 2. The two-dimensional correlation plot of ΔE vs E for identification of light charged particles. p, d, t, α denote proton, deuteron, triton, and alpha particles, respectively.

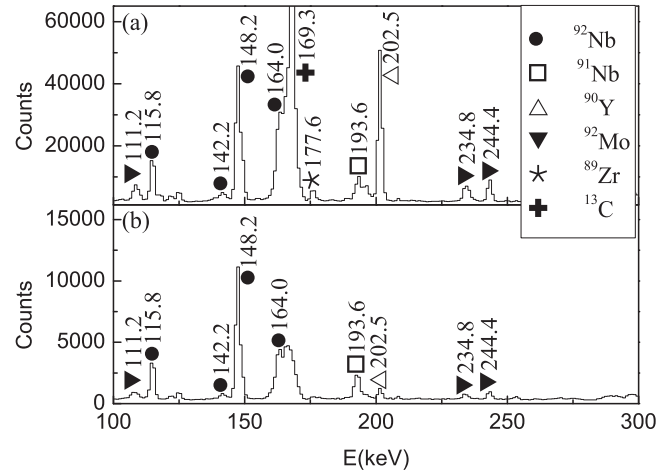

FIG. 3. The coincident γ-ray spectra with protons at angular ranges covered by the aluminum absorber (a) and unshielded by the aluminum absorber (b). ^{92}Mo and ^{89}Zr are from random coincidence with protons.

is usually assembled using silicon detectors with two shapes (hexagonal and pentagonal) to give the ΔE and E signals and covers about 0.2 steradian solid angle. Then the light charged particles can be identified by the two-dimensional matrix of ΔE and E. In addition, due to the reaction kinematics, five of 40 telescopes at most forward angles in the array are segmented into four sectors not only to sustain a higher counting rate but also to improve Doppler correction. The thicknesses of all ΔE and E detectors are 130 μm and 1000 μm, respectively. Each telescope is placed at distances around 6.5 cm from the target position.

An aluminum cylindrical absorber was inserted inside EUCLIDES and along the beam direction to protect the silicon detectors against the elastically scattered ions. The thickness of the absorber can be adjusted according to the beam-energy conditions and the reaction kinematics. In the commission of the ^{6}Li + ^{89}Y experiment, the thickness of cylinder was set 200 μm and the backward angles larger than 150° were unshielded by the absorber, see Fig. 1 for further details of the setup. A typical two-dimensional spectrum obtained at the angular ranges covered by the absorber at $E_{\rm lab} = 34$ MeV is shown in Fig. 2, in which protons, deuterons, tritons, and alphas labeled as p, d, t, and α can be clearly identified.

The data acquisition system (DAQ) is based on the XDAQ framework [55,56] to record the data. The average uncertainty (3%) of the efficiency and statistic of γ rays comes mainly from the standard radioactive sources and the least-squares fit method. The total uncertainty in this experiment for the values of the transfer cross sections comes from statistical errors associated with the yields of γ rays, and from systematic errors in the determination of the target thickness (1%), absolute efficiency, and beam intensity. The overall error is in the range from almost 7% at 34 MeV energy to 19% at 22 MeV energy.

III. DATA ANALYSIS AND RESULTS

In the ^{89}Y(^{6}Li,^{5}Li)^{90}Y* reaction, ^{90}Y is originated from one-neutron stripping process. However, in the region of medium-mass target, the fusion process evaporates not only neutrons, but also light charged particles including proton and α. Thus, the contribution from fusion process to the formation of ^{90}Y in the present system needs to be estimated.

We use the statistic evaporation code PACE4 to estimate the residuals of fusion of the ^{6}Li + ^{89}Y system. In this code the projectile energy, spins of projectile, and target nuclei are input. The defaulted value ($a = A/10$) of level density parameter was used. The main residues obtained from PACE calculations do not depend on the level density parameter even though the absolute values of the cross sections depend on it. According to the calculation results, in the ^{6}Li + ^{89}Y reaction, the ^{90}Y nucleus cannot be produced from the CF and ICF processes.

The charged-particle-γ coincidence method is also used to further confirm the formation of the ^{90}Y nucleus. Figure 3(a) shows the γ coincidence energy spectrum with protons from the angular ranges covered by the aluminum absorber at the incident energy of 34 MeV, where 202.5 keV γ line can be unambiguously observed. The 202.5 keV γ ray is one of the characteristic transitions of ^{90}Y. However, in Fig. 3(b) the 202.5 keV γ line almost disappears when selecting the proton particles from the angular ranges unshielded by the aluminum absorber where protons are emitted from the CF and ICF channels. This phenomenon is consistent with the fact that the protons detected in the angular ranges shielded by the aluminum absorber are originated from both transfer and fusion processes. On the contrary, the protons in the angular ranges unshielded by the aluminum absorber come mainly from the fusion process.

If the lifetimes of the excited states are much smaller than the irradiation time, the cross section for a certain channel can be obtained using in-beam γ-ray method. The cross sections of excited states can be determined as follows:

$$\sigma^{*}(E) = \frac{1}{N_B N_T}\left[\sum_{i=1}^{j}\frac{A_{E_{\gamma_i}}(E)}{\varepsilon_{E_{\gamma_i}}\varepsilon_d F_{E_{\gamma_i}}^{CE}}\right], \quad (1)$$

where i corresponds to the ith transition. $A_{E_{\gamma_i}}$ is the yield of the γ peak with energy E_{γ_i} at the bombarding energy E. $\varepsilon_{E_{\gamma_i}}$ is the absolute efficiency for the GALILEO γ ray with energy E_{γ_i}. ε_d is the correction factor for the dead time of the data acquisition

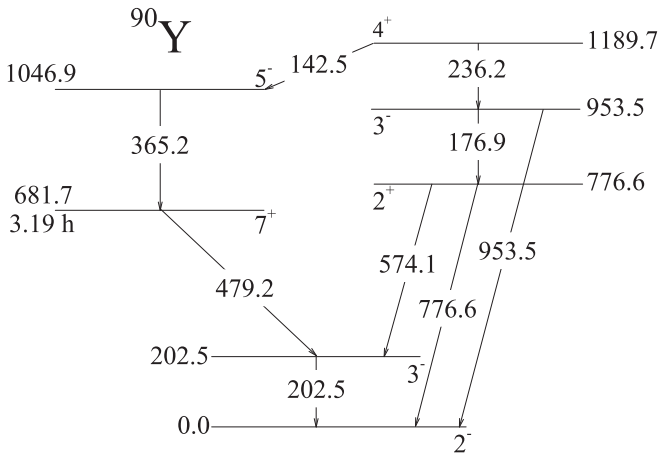

FIG. 4. The partial level scheme of ^{90}Y in the unit of keV [57].

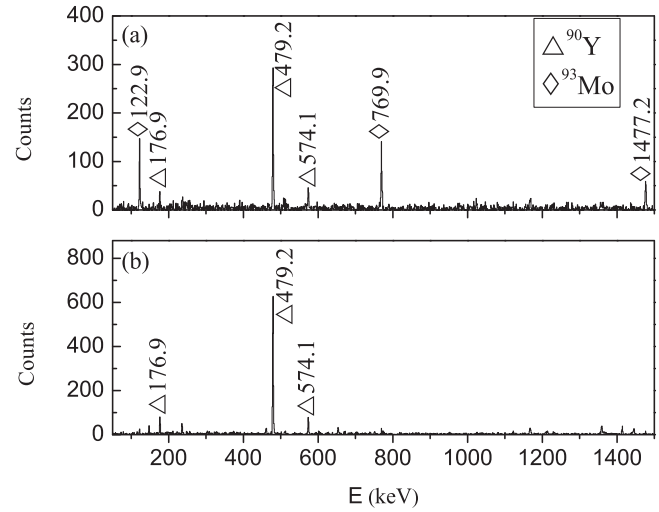

FIG. 5. The γ coincident energy spectra at 202.5 keV γ-gate condition at (a) 22 MeV and (b) 34 MeV.

system (DAQ). In this study, DAQ has no dead time, so $\varepsilon_d = 1$. $F^{CE}_{E\gamma_i}$ is the conversion electron correction for the $i \longrightarrow$ ground state (g.s.) transition. N_B and N_T are the total number of beam particles incident on the target and the target atoms per unit area, respectively.

For each transition, the accumulated number of counts during a run has to take into account the anisotropy of the emission and the detection efficiency, in such a way that one can write

$$A_{E_\gamma}(\theta) = N_{E_\gamma} F^{CE}_{E_\gamma} \varepsilon_{E_\gamma} \varepsilon_d W_{E_\gamma}(\theta), \tag{2}$$

where N_{E_γ} is the number of γ rays for the transition from the excited state to the ground state with energy E_γ, and W_{E_γ} is the angular distribution of γ rays emitted at the detection angle θ. W_{E_γ} is given by

$$W_{E_\gamma}(\theta) = 1 + \sum_{j=1}^{\infty} A_j(E_\gamma) P_j(\cos\theta), \tag{3}$$

where P_j is the Legendre polynomials of order j, and $A_j(E_\gamma)$ depends on the specific transition. Since the angular distributions of γ rays are symmetric along with 90°, in the present experiment the GALILEO array covers 90° and the backward angles (almost 2π space). Thus, the anisotropy of the γ emission does not need to be considered.

The partial level scheme of ^{90}Y is shown in Fig. 4 [57]. It can be clearly observed that there is a long-lived isomer in the ^{90}Y at 681.7 keV with a half-life of 3.19 (6) h. The existence of such long-lived isomer traps high-lying excited states from deexciting by γ transitions to lower-lying states in ^{90}Y. In data analysis, the in-beam and off-beam methods need to be used. In the in-beam analysis, the direct yields of the 3^- state at 202.5 keV in ^{90}Y is obtained by the intensity difference between 479.2 keV and 202.5 keV transitions. The coincident γ-ray spectra gated on 202.5 keV γ line with beam energy at 22 MeV and 34 MeV are shown in Figs. 5(a) and 5(b), respectively. Different cascades can be obviously observed. Figure 5(a) indicates the contaminant ^{93}Mo, which corresponds to 122.9 keV and 769.9 keV γ lines.

The same results can be estimated using PACE4. At 22 MeV the mainly evaporated residues include ^{93}Mo whose partial level scheme is shown in Fig. 6(a) [58]. One can see the 122.9 keV-203.0 keV-769.9 keV cascade of ^{93}Mo. When selecting the 122.9 keV γ ray as a gate condition, the coincident γ energy spectrum is shown in Fig. 6(b). The coincident 203.0 keV, 237.2 keV, 357.4 keV, 769.9 keV, 963.2 keV, 1477.2keV γ-ray lines are observed. Depending on this analysis, at 22 MeV the measured 202.5 keV γ rays are mainly contaminated by ^{93}Mo. From the yields of ^{90}Y directly populated on the 202.5 keV level should be subtracted the contribution of ^{93}Mo. Of course, the other contributions including the small contaminations may not be considered. So, the upper limit of the cross section of the 3^- state at 202.5 keV at 22 MeV is equal to (13.6 ± 1.8) mb. Using the same method the cross section of the 3^- state at 202.5 keV at 34 MeV can be determined.

In the off-beam analysis, the yields of isomer state at 681.7 keV and higher-lying states are calculated with the intensities of 479.2 keV and 202.5 keV transitions by off-beam decay

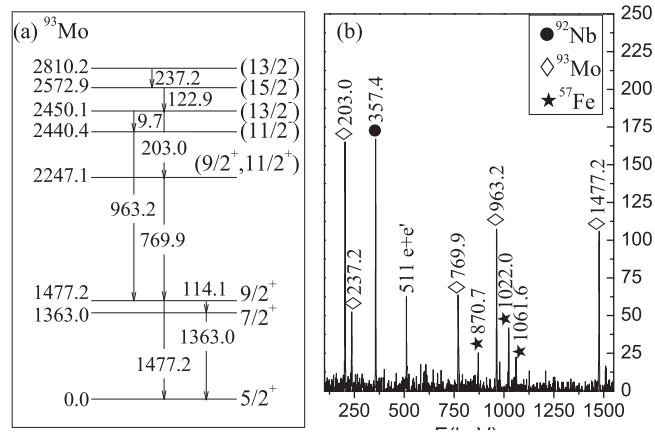

FIG. 6. (a) The partial level scheme of ^{93}Mo [58]; (b) The coincident γ spectrum with 122.9 keV γ-gate condition.

TABLE I. Comparison between experimental data and theoretical cross sections for the $^{5}Li_{g.s}(3/2^{-}) + {}^{90}Y_{g.s}(2^{-})$ and $^{5}Li_{g.s}(3/2^{-}) + {}^{90}Y^{*}$ channels. $^{90}Y^{*}$ corresponds to the sum of the contribution of the 3^{-} (0.202 MeV) and 7^{+} (0.681 MeV) states.

Final Partition	E_{lab} = 22 MeV Cross Sections (mb)		E_{lab} = 34 MeV Cross Sections (mb)	
	Exp.	Theo.	Exp.	Theo.
$^{5}Li_{g.s}(3/2^{-}) + {}^{90}Y_{g.s}(2^{-})$	–	23.2	–	18.3
$^{5}Li_{g.s}(3/2^{-}) + {}^{90}Y^{*}$	35.4 ± 6.8	34.0	25.5 ± 1.8	26.1

equation [12]. Thus the cross section of the isomer state at 681.7 keV and higher-lying states is equal to (21.8 ± 6.5) mb at 22 MeV. Finally, the total one-neutron stripping cross sections at 22 MeV and 34 MeV are equal to (35.4 ± 6.8) mb and (25.5 ± 1.8) mb, respectively. Here only the statistical error is considered.

The minimum neutron separation energy of ^{90}Y is 6.8 MeV. The separation energies for the other particles are also higher than 6 MeV. In our data analysis, all transitions feeding the ground state with the energy lower than 2 MeV ignore the probability of neutron emission, so only γ intensities are used to calculate the cross sections of the residues. We try to add all transitions that feed the ground state of ^{90}Y nucleus. However, due to the detection efficiency, the transitions whose energies are greater than 953.5 keV cannot be observed. We analyzed the transitions to the ground state from the high excited states (see Fig. 4). Using the single γ energy spectra, it was found that the intensity of these transitions corresponds to less than 5% of the total cross section. As a result, other transitions with intensity lower than this ratio are not considered due to the detection efficiency.

In comparison with $^{6}Li + {}^{96}Zr$ system, it is found that the derived one-neutron stripping cross sections for the $^{6}Li + {}^{89}Y$ system are much less than the CF cross sections for the $^{6}Li + {}^{96}Zr$ system [40] at energies above the Coulomb barrier. One-neutron stripping cross section for the $^{6}Li + {}^{89}Y$ system at 34 MeV is much less than that at 22 MeV. In comparison with one-neutron stripping cross sections for the $^{6}Li + {}^{96}Zr$ system [40], the cross section of the $^{6}Li + {}^{89}Y$ system has the same order of magnitude at energies around Coulomb barrier.

In Table I, the experimental and theoretical cross sections are compared, and although we have not experimental data for the $^{5}Li_{g.s}(3/2^{-}) + {}^{90}Y_{g.s}(2^{-})$ channel in the final partition, we did a theoretical prediction for it. One can observe that the cross section considering the ground state of the ^{90}Y is smaller than the one considering the sum of its excited states. This small suppression on the $^{5}Li_{g.s}(3/2^{-}) + {}^{90}Y_{g.s}(2^{-})$ cross section might be due to the Q value matching (the $Q_{g.s}$ = 1.19 MeV).

IV. THEORETICAL ANALYSIS OF THE $^{89}Y(^{6}Li,^{5}Li)^{90}Y$ REACTION

The theoretical cross section for the $^{89}Y(^{6}Li,^{5}Li_{g.s})^{90}Y^{*}$ reaction was obtained by performing coupled reaction channels (CRC) calculations, where the $^{90}Y^{*}$ corresponds to the sum of the contribution of the 3^{-} (0.202 MeV) and 7^{+} (0.681 MeV) states. The São Paulo double folding potential [59] was used as optical potential in both real and imaginary parts [$U = (1.0 + N_I)V_{SP}$], where N_I stands for the strength coefficient of the imaginary part of the optical potential. The ^{6}Li is a weakly bound nucleus and it can be broken into $^{4}He + d$ by its interaction with the target. As we are not explicitly considering the coupling to continuum states due to the breakup mechanism, the imaginary part of the optical potential in the entrance partition was multiplied by strength coefficient $N_I = 0.6$. This coefficient is able to account for the loss of flux to dissipative channels including the breakup channel, according to Refs. [60,61]. On the other hand, in the outgoing partition, the imaginary part was multiplied by strength coefficient $N_I = 0.78$, as soon as no coupling was explicitly considered. This procedure has been shown to be suitable for describing the elastic scattering cross section for many systems in a wide energy interval [62]. To generate the single-particle wave function, Woods-Saxon potentials were used and the reduced radius and diffuseness were set to 1.25 fm and 0.65 fm, respectively, for both the ^{6}Li projectile and the ^{89}Y target. The depths of the Woods-Saxon potentials were varied in order to fit the experimental one-neutron binding energies. Besides that, the collective states of the target were taken into account in the CRC calculation as shown in the coupling scheme of Fig. 7. The electrical reduced transitions probabilities for the collective excitation for ^{89}Y were obtained from Ref. [63]. Another important ingredient to perform microscopic CRC calculation is the spectroscopic amplitudes for the projectile and target overlaps. These spectroscopic amplitudes were derived performing shell-model calculations with the NUSHELLX code [64]. To obtain the one-neutron spectroscopic information of the target overlaps, the *sn* model space and effective interaction *snt* were used. In this model

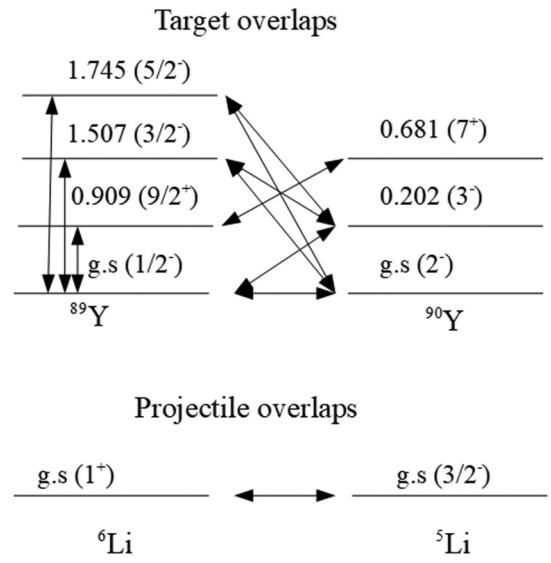

FIG. 7. Coupling scheme considered in the one-neutron transfer calculation.

TABLE II. Spectroscopic amplitudes used in the CRC calculations for one-neutron transfer reactions, where j is the spin of the neutron orbitals.

Initial State	j	Final State	Spect. Ampl.
$^{89}Y_{g.s}(1/2^-)$	$(2d_{5/2})$	$^{90}Y_{g.s}(2^-)$	0.993
$^{89}Y_{g.s}(1/2^-)$	$(2d_{5/2})$	$^{90}Y_{0.202}(3^-)$	0.993
	$(1g_{7/2})$		0.00001
	$(2d_{5/2})$		−0.990
$^{89}Y_{0.909}(9/2^+)$	$(1g_{9/2})$	$^{90}Y_{0.681}(7^+)$	0.068
	$(1g_{7/2})$		0.052
$^{89}Y_{1.507}(3/2^-)$	$(2d_{5/2})$	$^{90}Y_{g.s}(2^-)$	0.017
	$(1g_{7/2})$		−0.031
	$(2d_{5/2})$		−0.010
$^{89}Y_{1.507}(3/2^-)$	$(1g_{7/2})$	$^{90}Y_{0.202}(3^-)$	0.039
	$(1g_{9/2})$		0.752
	$(2d_{5/2})$		−0.026
$^{89}Y_{1.745}(5/2^-)$	$(1g_{7/2})$	$^{90}Y_{gs}(2^-)$	0.016
	$(1g_{9/2})$		−0.159
	$(2d_{5/2})$		0.002
$^{89}Y_{1.745}(5/2^-)$	$(1g_{7/2})$	$^{90}Y_{0.202}(3^-)$	0.023
	$(1g_{9/2})$		0.911

space the ^{56}Ni nucleus is considered as closed core and the $1f_{5/2}, 2p_{3/2}, 2p_{1/2}, 1g_{9/2}, 1g_{7/2}, 2d_{5/2}, 2d_{3/2}$, and $3s_{1/2}$ orbitals are taken as the valence space for the neutrons and protons. Due to our computational limitations in performing shell-model calculations, using that large valence space, it was necessary to introduce some constrains to derive the amplitudes. Therefore, instead of ^{56}Ni, the ^{84}Sr nucleus was considered as a closed core and only the $1g_{9/2}$, $1g_{7/2}$, and $2d_{5/2}$ orbitals were included in the neutron valence subspace and the $2p_{1/2}$ and $1g_{9/2}$ orbitals for the proton valence space. For the projectile overlaps, the same spectroscopic amplitude considered in Ref. [40] was used. In Table II, the spectroscopic amplitudes used in the one-neutron transfer calculation concerning to the target overlaps are shown. In Fig. 8, the theoretical predictions on the energy interval from 18–36 MeV are shown. The experimental cross sections at 22 and 34 MeV for the $^5Li_{g.s} + {}^{90}Y^*$ channel are also shown. Despite the constraints imposed to the model space, it is possible to observe a good agreement between the CRC results and the data, which is an indication that the relevant single-particle wave functions are being taken into account. These constraints mainly affect the overlaps of the $^{89}Y_{0.909}(9/2^+)$ with both $^{90}Y_{gs}(2^-)$ and $^{90}Y_{0.202}(3^-)$ states because the $2p_{3/2}$ and $1f_{5/2}$ orbitals were not considered in the valence space. Nevertheless, in order to verify the relevance of these missing couplings, we included the $9/2^+$ of ^{89}Y at 0.909 MeV and considered spectroscopic amplitudes for the overlaps mentioned above equal to 1.0. The inclusion of these overlaps produces vanishing effect on the cross sections of the one-neutron transfer to the $^{90}Y^*$. For the overlaps between $^{89}Y_{1.507}(3/2^-)$ and $^{89}Y_{1.745}(5/2^-)$ with $^{90}Y_{0.681}(7^+)$ state, the spectroscopic amplitudes could be obtained if the $1h_{11/2}$ orbital is considered. In order to check the effect of those overlaps in the one-neutron transfer process, we included them in the CRC calculations considering spectroscopic amplitudes equal to 1.0. Again, the effect of the new overlaps was found completely negligible.

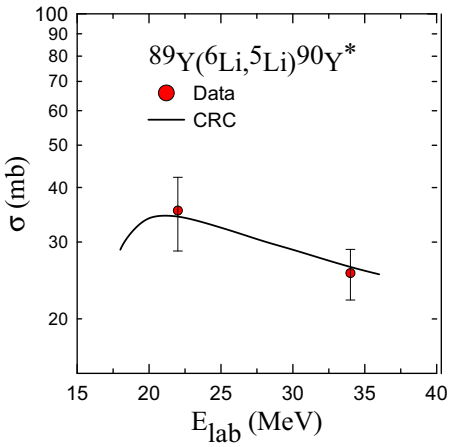

FIG. 8. Comparison between the theoretical results and experimental data of the cross sections of one-neutron stripping reaction.

From Fig. 8, it can be seen that the one-neutron transfer excitation function increases until energies around the Coulomb barrier, and then starts to drop slowly for energies above the barrier. Indeed, at incident energies below the barrier, the one-neutron transfer cross section decreases because it is a reaction mechanism with a threshold, given by the conservation of the energy. It might be higher than the fusion cross section because it is a direct peripheral process that does not depend on the penetration of the Coulomb barrier. Other processes such as the breakup, Coulomb (mainly) collective excitation, and the breakup channel may remain also opened at energies below the Coulomb barrier. At energies above the Coulomb barrier, many reaction channels are opened, and they are caused not only by the Coulomb interaction but also by nuclear interactions. Strong interference between Coulomb and nuclear interactions and among different reaction mechanisms occurs, and the slope of the excitation function depends on the structure of the reacting nuclei and the mechanisms opened at this energy regime.

V. DISCUSSIONS

Although there is no experimental data available for the fusion cross section or the elastic scattering of the $^6Li + {}^{89}Y$ reaction, it is important to perform calculations to study the effect of one-neutron stripping channel on these reaction mechanisms. It is important to mention that the breakup channel will not be considered in our theoretical calculations, although it is expected that both the elastic and the fusion cross sections should be affected by the breakup channel. Our main objective is to disentangle the effect of the one-neutron stripping process on other reaction mechanisms. This is a very important aspect when the main conclusions found in the literature about the effect of the breakup channel on other reaction mechanisms (such as fusion) are entangled with transfer effect [1,2,9–16].

Coupled channel (CC) calculations were performed in which the only difference from the previous CRC calculations is that the one-neutron stripping channel was switched off. This

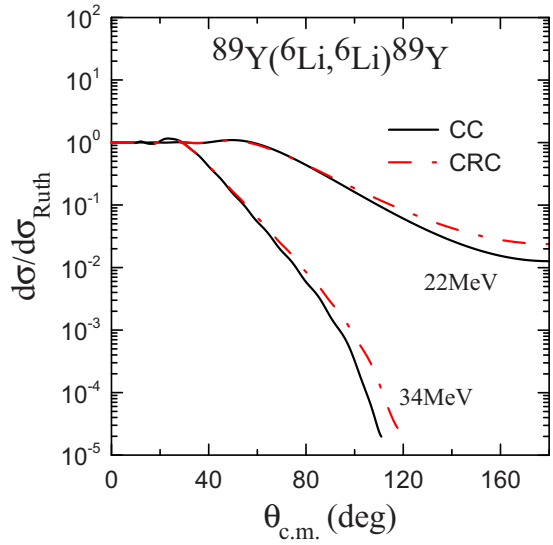

FIG. 9. Comparison of CC and CRC results for the elastic scattering at 22 MeV and 34 MeV.

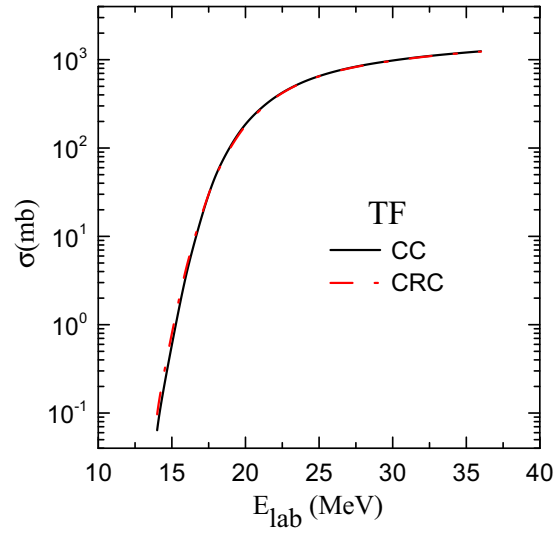

FIG. 10. Comparison of CC and CRC results for total fusion cross section at energies near the barrier.

is the way we will verify the exclusive influence of the neutron transfer channel on the total fusion and the elastic scattering processes.

In Fig. 9, the results of CC and CRC calculations for the elastic scattering angular distributions are compared for the same two energies for which the transfer reaction was measured and discussed in the previous sections. One can see that the one-neutron stripping reaction has a considerable influence on the elastic scattering angular distributions at angles larger than the one corresponding to the main Fresnel peak or the so-called Coulomb rainbow peak. The effect is to increase the elastic scattering in the region where the nuclear interactions are important, and consequently to decrease the reaction cross section.

In Fig. 10, the comparison of the total fusion cross section obtained from CC and CRC calculations is shown. The energy range of the calculations from 14–36 MeV covers the two energies for which the neutron transfer reaction was measured, and includes energies below and above the Coulomb barrier. As one can see from this figure, the results of both calculations almost coincide in the whole energy interval meaning that the effect of the one-neutron stripping transfer channel on the fusion is completely negligible for this system. This result is in agreement with recent results found for the effect of the neutron transfer channel on the fusion of the ^{7}Li + ^{119}Sn system [39], where a negligible effect was also found. Of course, this is not a general result. There might be other systems for which the one-neutron transfer affects the fusion. It has been shown that the neutron transfer reaction may trigger breakup reactions for some systems at energies below the Coulomb barrier [33–36]. For the ^{6}Li + ^{89}Y system, it seems that this kind of process may not be relevant, even at energies below the Coulomb barrier. However, to support this conclusion more detailed studies from both theoretical and experimental point of view are necessary. The experimental fusion cross section has to be measured, and sequential breakup calculations, such as the one performed in Ref. [65], have to be performed. This kind of calculation is out of the scope of the present work.

To finish this section we would like to discuss in detail the sensibility of our results for the one-neutron transfer cross section to the choice of two free parameters: the reduced radius and the diffuseness of the Woods-Saxon form factors. As it has been stated in the previous section, in our CRC calculations we used the parameter-free São Paulo potential as optical potential. However, to generate the single-particle states, Woods-Saxon form factors were used for both projectile and target overlaps. This kind of potential has three parameters: the depth, the reduced radius, and the diffuseness. Usually, one fixes the latter two parameters (the geometrical parameters) and varies the depth in order to fit the experimental binding energy. This potential is directly related to the calculation of the transfer amplitudes because it is used as part of the interaction Hamiltonian between the colliding nuclei. Thus, it is important to study the sensibility of the transfer cross section to the increment or decrement of the reduced radius and diffuseness of the projectile and the target form factors.

In Fig. 11, the sensibility of the transfer cross section to the variation of the Woods-Saxon geometrical parameters is shown. Figure 11(a) shows the results when the parameters of both projectile and target form factors were increased or decreased at the same time. The reduced radii were increased to 1.3 fm and decreased to 1.2 fm, while diffusenesses were increased to 0.7 fm and decreased to 0.6 fm. This is a typical range of the values found in the literature for nuclei not having special structure characteristics, such as neutron skin or halo structure. One can see that increasing (decreasing) both parameters at the same time for the form factor of the projectile and target produces the same effect of increasing (decreasing) the transfer cross section (as expected) in a symmetric way when compared to the result with mean values for these geometrical parameters.

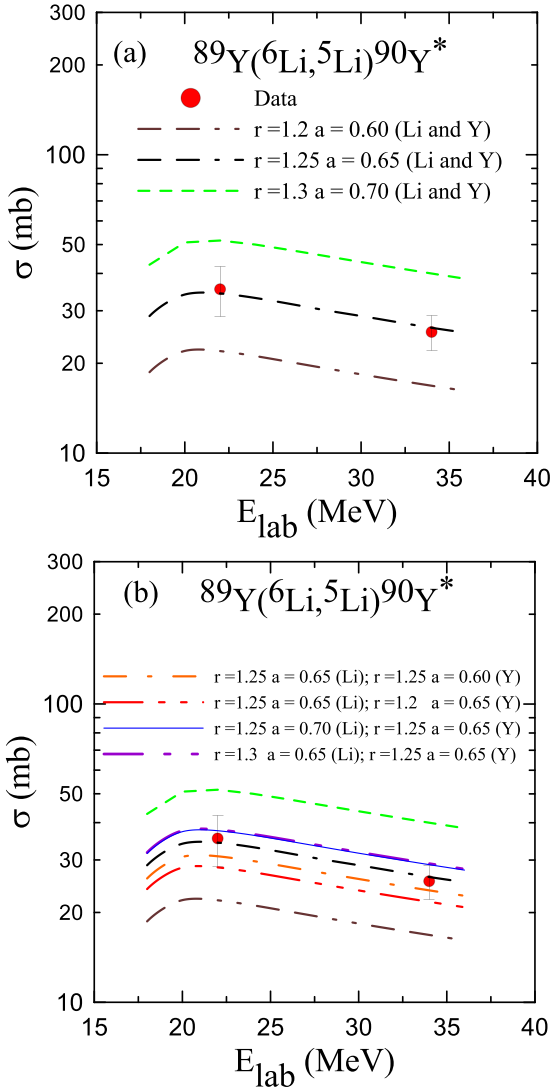

FIG. 11. Sensibility of the one-neutron transfer reaction to the variation of the reduced radius and diffuseness of the form factor of the projectile and target overlaps. The reduced radii and diffuseness are given in fm.

In Fig. 11(b) the separate effect of the variation of the geometrical parameters of the projectile and target form factors is studied. Therefore, first, we increased the diffuseness of the projectile potential (solid thin line) and then the increased-only reduced radius (dash-dot-dot line). The result when the diffuseness of the target potential is decreased is represented by the dash-dot line, while the dash-dot-dot-dot one represents the result when only the reduced radius is decreased. One can see that the change in the reduced radius and diffuseness produces the same effect in the case of the projectile and that the cross sections are more sensitive to the changes on the geometrical parameters of the target form factor, especially on its reduced radius.

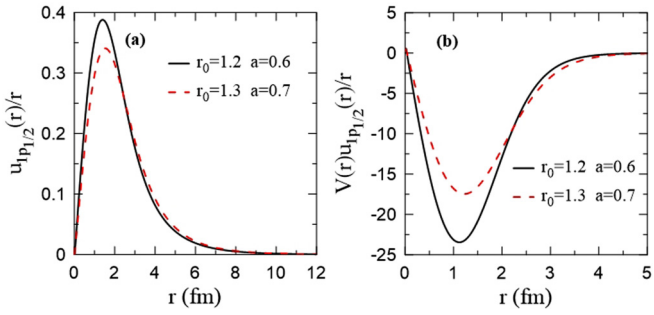

FIG. 12. Wave function and potential overlap for the $\langle^5\mathrm{Li}(3/2^-)|^6\mathrm{Li}(1^+)\rangle$ overlap with binding energy $BE = -5.664$ MeV.

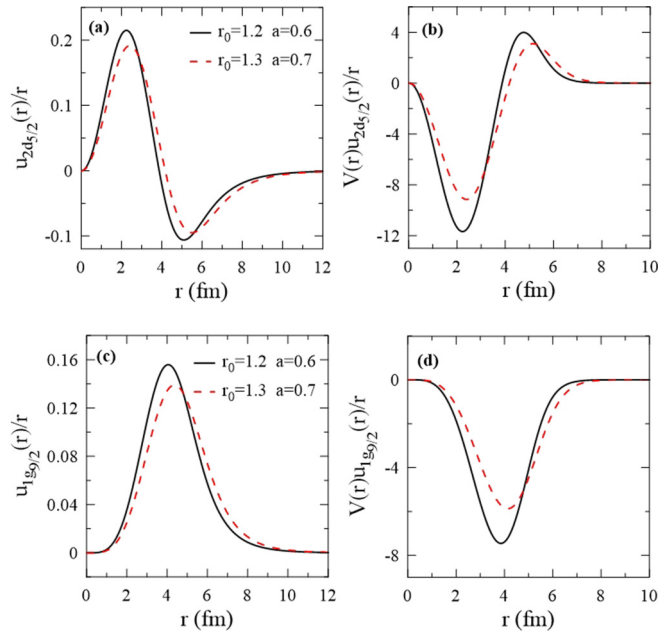

FIG. 13. Wave function and potential overlap for the $\langle^{89}\mathrm{Y}(1/2^-)|^{90}\mathrm{Y}(3^-)\rangle$ overlap with binding energy $BE = -6.655$ MeV (top), and for the $\langle^{89}\mathrm{Y}(3/2^-)|^{90}\mathrm{Y}(3^-)\rangle$ overlap with binding energy $BE = -8.162$ MeV (bottom).

In Fig. 12 we show the wave function [u(r)/r] and potential overlap [V(r)u(r)/r] for the $\langle^5\mathrm{Li}(3/2^-)|^6\mathrm{Li}(1^+)\rangle$ projectile's g.s. overlap. Figure 13 shows similar results for the $\langle^{89}\mathrm{Y}(1/2^-)|^{90}\mathrm{Y}(3^-)\rangle$ (top panel) and $\langle^{89}\mathrm{Y}(3/2^-)|^{90}\mathrm{Y}(3^-)\rangle$ (bottom panel) target overlaps. From these two figures, it is clearly visible that changes in the geometrical parameter of the form factors produce larger changes on the wave functions of the target than on that of the projectile in agreement with the conclusions taken from Fig. 11.

So, although some effects of the geometrical parameters of the target form factor on the absolute value of the one-neutron stripping cross section are observed, they are not so dramatic. Typical values of the reduced radius and diffuseness (i.e., 1.25 fm and 0.65 fm, respectively) guarantee good agreement with the experimental data.

VI. SUMMARY

The experiment for the study of $^6\mathrm{Li} + ^{89}\mathrm{Y}$ reaction has been performed on GALILEO array coupled with 4π Si-ball EUCLIDES at Legnaro National Laboratory. We have measured the cross sections for the one-neutron stripping from

^{6}Li to the ^{89}Y target, feeding excited states of ^{90}Y, by the in-beam and off-beam γ-ray spectroscopy methods at 22 MeV and 34 MeV beam energies. ^{90}Y is verified from one-neutron stripping process by protons-γ rays coincidence method. Since it is not possible to determine the cross section for feeding the ground state of ^{90}Y by the in-beam γ spectroscopy method, the presently obtained cross sections are part of the one-neutron stripping cross section. At energies above the Coulomb barrier, the derived cross sections are much less than the CF cross sections for the ^{6}Li + ^{96}Zr system and keep the same order of magnitude with one-neutron stripping cross sections of ^{6}Li + ^{96}Zr at energies around the Coulomb barrier. The theoretical cross section for the ^{89}Y(^{6}Li,^{5}Li$_{g.s}$)^{90}Y* reaction was calculated by using the coupled reaction channels approach, in which the ^{90}Y* corresponds to the sum of the contribution of the 3^{-} (0.202) and 7^{+} (0.681) states. The theoretical cross sections are in a good agreement with experimental data. An extrapolation of this trend results in a conclusion that the transfer cross section should predominate over CF cross sections at sub-barrier energies. These phenomena correspond to two different reaction mechanisms. The neutron transfer process does not need to tunnel a Coulomb barrier, as it does in the case of the fusion process. Therefore, when one deals with reactions with weakly bound nuclei, even neutron-halo nuclei, the neutron transfer reaction may contribute significantly to the total cross section at energies close to and below the Coulomb barrier.

A pure theoretical analysis showed that while the one-neutron stripping reaction affects the elastic scattering angular distribution, and consequently the reaction cross section, it does not affect the TF cross section, even at energies below the Coulomb barrier. So, it might be expected that the effect of transfer plus breakup reported usually in the literature on the fusion cross section might be related exclusively to the breakup mechanism for this system. It would be important to corroborate this conclusion with the experimental data for fusion reactions (TF and CF) for this system.

ACKNOWLEDGMENTS

We are grateful to the INFN-LNL staff for providing stable ^{6}Li beam throughout the experiment. This work is supported by the National Nature Science Foundation of China under Grants No. 11475013, No. 11375266, No. 11605114, No. 11575118, and No. 11505117 as well as the National Natural Science Foundation of Guangdong, China (2016A030310042) and the National Key Research and Development Program of China, the National Key Scientific Instrument and Equipment Development Projects, China (2017YFF0106501). The Brazilian authors thank CNPq, CAPES, and FAPERJ for the partial financial support through the research project INCT-FNA Proc. No 464898/2014-5.

G.L.Z. and G.X.Z. contributed equally to this work.

[1] L. F. Canto, P. R. S. Gomes, R. Donangelo, J. Lubian, and M. S. Hussein, Phys. Rep. **596**, 1 (2015).
[2] L. F. Canto, P. R. S. Gomes, R. Donangelo, and M. S. Hussein, Phys. Rep. **424**, 1 (2006).
[3] G. L. Zhang, C. L. Zhang, H. Q. Zhang *et al.*, Eur. Phys. J. A **48**, 65 (2012).
[4] B. B. Back, H. Esbensen, C. L. Jiang, and K. E. Rehm, Rev. Mod. Phys. **86**, 317 (2014).
[5] N. Keeley, R. Raabe, N. Alamanos, and J. J. Sida, Prog. Part. Nucl. Phys. **59**, 579 (2007).
[6] N. Keeley, N. Alamanos, K. W. Kemper, and K. Rusek, Prog. Part. Nucl. Phys. **63**, 396 (2009).
[7] J. F. Liang and C. Signorini, Int. J. Mod. Phys. E **14**, 1121 (2005).
[8] K. Hagino and N. Takigawa, Prog. Theor. Phys. **128**, 1061 (2012).
[9] S. P. Hu, G. L. Zhang, J. C. Yang *et al.*, Phys. Rev. C **91**, 044619 (2015).
[10] C. L. Guo, G. L. Zhang, S. P. Hu *et al.*, Phys. Rev. C **92**, 014615 (2015).
[11] Y. D. Fang, P. R. S. Gomes, J. Lubian *et al.*, Phys. Rev. C **91**, 014608 (2015).
[12] N. T. Zhang, Y. D. Fang, P. R. S. Gomes *et al.*, Phys. Rev. C **90**, 024621 (2014).
[13] P. R. S. Gomes, J. Lubian, and L. F. Canto, Phys. Rev. C **79**, 027606 (2009).
[14] H. Kumawat, V. Jha, V. V. Parkar *et al.*, Phys. Rev. C **86**, 024607 (2012).
[15] M. K. Pradhan, A. Mukherjee, P. Basu *et al.*, Phys. Rev. C **83**, 064606 (2011).
[16] B. Wang, W. J. Zhao, P. R. S. Gomes, E. G. Zhao, and S. G. Zhou, Phys. Rev. C **90**, 034612 (2014)
[17] A. Diaz-Torres and I. J. Thompson, Phys. Rev. C **65**, 024606 (2002).
[18] K. Hagino, A. Vitturi, C. H. Dasso, and S. M. Lenzi, Phys. Rev. C **61**, 037602 (2000).
[19] J. Lubian *et al.*, Nucl. Phys. A **791**, 24 (2007).
[20] J. Lubian, T. Correa, E. F. Aguilera, L. F. Canto, A. Gomez-Camacho, E. M. Quiroz, and P. R. S. Gomes, Phys. Rev. C **79**, 064605 (2009).
[21] S. Santra, S. Kailas, K. Ramachandran, V. V. Parkar, V. Jha, B. J. Roy, and P. Shukla, Phys. Rev. C **83**, 034616 (2011).
[22] M. A. Nagarajan, C. C. Mahaux, and G. R. Satchler, Phys. Rev. Lett. **54**, 1136 (1985).
[23] C. C. Mahaux, H. Ngô, and G. R. Satchler, Nucl. Phys. A **449**, 354 (1986).
[24] G. R. Satchler, Phys. Rep. **199**, 147 (1991).
[25] M. E. Brandan and G. R. Satchler, Phys. Rep. **285**, 143 (1997).
[26] C. J. Lin, J. C. Xu, H. Q. Zhang, Z. H. Liu, F. Yang, and L. X. Lu, Phys. Rev. C **63**, 064606 (2001)
[27] M. S. Hussein, P. R. S. Gomes, J. Lubian, and L. C. Chamon, Phys. Rev. C **73**, 044610 (2006)
[28] V. V. Parkar, V. Jha, S. K. Pandit, S. Santra, and S. Kailas, Phys. Rev. C **87**, 034602 (2013).
[29] N. Keeley, N. Alamanos, K. Rusek, and K. W. Kemper, Phys. Rev. C **71**, 014611 (2005).
[30] D. S. Monteiro, O. A. Capurro, A. Arazi *et al.*, Phys. Rev. C **79**, 014601 (2009).

[31] H. M. Jia, C. J. Lin, H. Q. Zhang *et al.*, Phys. Rev. C **82**, 027602 (2010).
[32] C. L. Jin *et al.*, Nucl. Phys. A **787**, 281 (2007).
[33] R. Rafiei, R. du Rietz, D. H. Luong, D. J. Hinde, M. Dasgupta, M. Evers, and A. Diaz-Torres, Phys. Rev. C **81**, 024601 (2010).
[34] D. H. Luong *et al.*, Phys. Lett. B **695**, 105 (2011).
[35] D. H. Luong, M. Dasgupta, D. J. Hinde, R. duRietz, R. Rafiei, C. J. Lin, M. Evers, and A. Diaz-Torres, Phys. Rev. C **88**, 034609 (2013).
[36] E. C. Simpson, K. J. Cook, D. H. Luong, S. Kalkal, I. P. Carter, M. Dasgupta, D. J. Hinde, and E. Williams, Phys. Rev. C **93**, 024605 (2016).
[37] A. Shrivastava *et al.*, Phys. Lett. B **633**, 463 (2006).
[38] S. Santra *et al.*, Phys. Lett. B **677**, 139 (2009).
[39] M. Fisichella, A. C. Shotter, P. Figuera, J. Lubian, A. DiPietro, J. P. Fernandez-Garcia, J. L. Ferreira, M. Lattuada, P. Lotti, A. Musumarra, M. G. Pellegriti, C. Ruiz, V. Scuderi, E. Strano, D. Torresi, and M. Zadro, Phys. Rev. C **95**, 034617 (2017).
[40] S. P. Hu, G. L. Zhang, J. C. Yang *et al.*, Phys. Rev. C **93**, 014621 (2016).
[41] Y. D. Fang, P. R. S. Gomes, J. Lubian *et al.*, Phys. Rev. C **93**, 034615 (2016).
[42] A. Shrivastava, A. Navin, A. Lemasson, K. Ramachandran, V. Nanal, M. Rejmund, K. Hagino, T. Ichikawa, S. Bhattacharyya, A. Chatterjee, S. Kailas, K. Mahata, V. V. Parkar, R. G. Pillay, and P. C. Rout, Phys. Rev. Lett. **103**, 232702 (2009).
[43] A. Shrivastava *et al.*, Phys. Lett. B **718**, 931 (2013).
[44] C. S. Palshetkar, S. Thakur, V. Nanal, A. Shrivastava, N. Dokania, V. Singh, V. V. Parkar, P. C. Rout, R. Palit, R. G. Pillay, S. Bhattacharyya, A. Chatterjee, S. Santra, K. Ramachandran, and N. L. Singh, Phys. Rev. C **89**, 024607 (2014).
[45] A. Di Pietro, P. Figuera, E. Strano, M. Fisichella, O. Goryunov, M. Lattuada, C. Maiolino, C. Marchetta, M. Milin, A. Musumarra, V. Ostashko, M. G. Pellegriti, V. Privitera, G. Randisi, L. Romano, D. Santonocito, V. Scuderi, D. Torresi, and M. Zadro, Phys. Rev. C **87**, 064614 (2013).
[46] D. J. Hinde, M. Dasgupta, B. R. Fulton, C. R. Morton, R. J. Wooliscroft, A. C. Berriman, and K. Hagino, Phys. Rev. Lett. **89**, 272701 (2002).
[47] C. Signorini, Eur. Phys. J. A **13**, 129 (2002).
[48] A. Chatterjee, A. Navin, A. Shrivastava, S. Bhattacharyya, M. Rejmund, N. Keeley, V. Nanal, J. Nyberg, R. G. Pillay, K. Ramachandran, I. Stefan, D. Bazin, D. Beaumel, Y. Blumenfeld, G. deFrance, D. Gupta, M. Labiche, A. Lemasson, R. Lemmon, R. Raabe, J. A. Scarpaci, C. Simenel, and C. Timis, Phys. Rev. Lett. **101**, 032701 (2008).
[49] A. Lemasson, A. Shrivastava, A. Navin, M. Rejmund, N. Keeley, V. Zelevinsky, S. Bhattacharyya, A. Chatterjee, G. deFrance, B. Jacquot, V. Nanal, R. G. Pillay, R. Raabe, and C. Schmitt, Phys. Rev. Lett. **103**, 232701 (2009).
[50] R. Raabe *et al.*, Nature (London) **431**, 823 (2004).
[51] J. J. Valiente-Dobón *et al.*, INFN-LNL Annual Report No. 95, 2014.
[52] D. Testov *et al.*, INFN-LNL Annual Report No. 105, 2015.
[53] A. Gadea *et al.*, INFN-LNL Annual Report No. 225, 1996.
[54] A. Gadea *et al.*, INFN-LNL Annual Report No. 118, 1997.
[55] J. Gutleber, S. Murray, and L. Orsini, Comput. Phys. Commun. **153**, 155 (2003).
[56] D. Barientos, L. Berti, M. Biasotto, S. Fantinel, A. Gozzelino, M. Gulmini, and N. Toniolo, IEEE Trans. Nucl. Sci. **62**, 3134 (2015).
[57] S. Michaelsen, A. Harder, K. P. Lieb, G. Graw, R. Hertenberger, D. Hofer, P. Schiemenz, E. Zanotti, H. Lenske, A. Weigel, H. H. Wolter, S. J. Robinson, and A. P. Williams, Nucl. Phys. A **552**, 232 (1993).
[58] S. Mitarai and E. Minehara, Nucl. Phys. A **406**, 55 (1983).
[59] L. C. Chamon, D. Pereira, M. S. Hussein, M. A. Candido Ribeiro, and D. Galetti, Phys. Rev. Lett. **79**, 5218 (1997).
[60] D. Pereira, J. Lubian, J. R. B. Oliveira, D. P. de Souza, and L. C. Chamon, Phys. Lett. B **670**, 330 (2009).
[61] D. P. Souza, D. Pereira, J. Lubian, L. C. Chamon, J. R. B. Oliveira, E. S. Rossi Jr., C. P. Silva, P. N. de Faria, V. Guimarães, R. Lichtenthaler, and M. A. G. Alvarez, Nucl. Phys. A **836**, 1 (2010).
[62] L. R. Gasques, L. C. Chamon, P. R. S. Gomes, and J. Lubian, Nucl. Phys. A **764**, 135 (2006).
[63] J. E. Wise *et al.*, Phys. Rev. C **42**, 1077 (1990).
[64] W. D. M. Rae, http://www.garsington.eclipse.co.uk (2008).
[65] D. R. Otomar *et al.*, J. Phys. G: Nucl. Part. Phys. **40**, 125105 (2013).